The Effect of High-Temperature Eutectic-Forming Impurities on Aluminum 7108 Weldability

Iron and other similar transition impurity elements can form high melting temperature eutectics that can affect weldability, grain size, and interdendritic feeding

BY M. G. MOUSAVI, C. E. CROSS, AND Ø. GRONG

ABSTRACT

The weldability of the 7108 aluminum extrusion alloy has been found to exhibit a high sensitivity to iron impurity content. This is believed to be related to the formation of a high-melting-temperature Al-Fe eutectic, capable of blocking interdendritic fluid flow and impeding the feeding of solidification shrinkage and thermal strain. Other high-temperature, eutectic-forming impurities have been found to behave in a similar manner when added to Alloy 7108 in a controlled manner. The circular patch test (CPT) was adapted to evaluate the effect of impurity elements on the solidification cracking susceptibility of welds made on cast 7108 coupons, treated with different impurity metal additions. Results from the CPT have shown a correlation between the amount of eutectic generated, as predicted using the Scheil Equation, and the susceptibility to cracking. However, in some instances, impurities are also observed to refine the grain size, an effect that tends to counteract their negative influence on weldability.

Introduction

Weldable 7xxx alloys were developed in the 1960s as a high-strength alternative to weldable 5xxx alloys (e.g., Alloy 5083). These are basically Al-Mg-Zn alloys that are copper free and respond well to natural aging in the weld metal and heat-affected zone (HAZ) following welding (e.g., Alloys 7039, 7005, and 7108). The copper-containing 7xxx alloys (e.g., Alloy 7075) constitute high-strength aerospace alloys and are generally not considered weldable.

Alloy 7108 is one such Al-Mg-Zn precipitation-hardenable extrusion alloy (Al-5½Zn+1Mg), considered to be readily weldable when using an appropriate filler alloy such as Alloy 5183 (Al-5Mg). The high zinc in the base metal, when diluted with the high magnesium in the filler metal, shifts the composition of the weld metal away from the region of highest cracking susceptibility (Ref. 1). From the standpoint of maintaining high strength, however, it is preferable to minimize the amount of filler dilution and keep the weld metal zinc content high (Ref. 2).

During a circular patch test (CPT) study examining the autogenous weldability of different alloy variations of 7108, it was discovered that high-purity variants exhibited no tendency toward cracking (Ref. 3). Whereas, the same test applied to a commercial 7108 alloy resulted in severe cracking. This led to a suspicion of the role of impurity elements and their influence on weldability. Alloy 7108 normally contains up to 0.25 wt-% Fe, 0.12 wt-% Si, and 0.04 wt-% Mn as acceptable impurity levels (Ref. 4). The impurities Fe and Si, in particular, are common to all commercial aluminum alloys as residuals from the extractive processing of aluminum ore.

The present study was specifically initiated to systematically investigate how Fe impurity levels affect the weldability of Alloy 7108. Other transition elements that form a high-melting eutectic similar to Fe (i.e., Sc, Mn, Co, and Ni) were also examined in order to provide a basis for comparison. Data regarding the effect of Sc, although not specifically generated for this study, have been drawn from previous work (Ref. 5). Such comparisons become important when developing mechanistic models to explain observed behavior. The role of Si, an impurity normally found together with Fe, was not addressed in this study. However, it is recognized that the presence of Si, and its tendency to form intermetallics with Fe, has the potential to alter the effect of Fe on weldability.

KEYWORDS

Sc, Mn, Fe, Co, and Ni
Alloy 7108
Eutectic
Interdendritic Fluid Flow
Weldability
Grain Size
Circular Patch Test (CPT)

Background

Transition Element Phase Equilibrium

Fe sits in the first row of the transition elements in the periodic table and, just like its neighbors Sc, Mn, Co, and Ni, it forms a high-melting eutectic with aluminum at the aluminum-rich end of the binary phase diagram — Fig. 1. On the other hand, the transition elements Ti, V, and Cr all form peritectics with aluminum (as do all the elements in these three columns: IVB, VB, and VIB). It is interesting to note that Ti, V, and Zr (Zr lies below Ti on the periodic table) are often added to aluminum alloys for grain refinement, because the peritectic reaction ($L + \beta \rightarrow \alpha$) provides an ideal nucleating substrate (Ref. 6). However, Sc has also been found to result in grain refinement even though it is not a peritectic former, presumably because the eutectic $ScAl_3$ compound favors the nucleation of aluminum grains (Refs. 5, 7).

The eutectic-forming transition elements shown in Fig. 1 all involve the formation of an intermetallic compound with aluminum at relatively high temperatures (see Table 1). Sc and Fe form a binary eutectic with aluminum at 655°C, Mn and Co form a eutectic at 657°C, and Ni forms a eutectic at 640°C. The eutectic tempera-

M. G. MOUSAVI is with the Department of Technology, University College of Buskerud, Kongsberg, Norway; C. E. CROSS (carl-edward.cross@bam.de) *is with the Division for Safety of Joined Components, Federal Institute for Materials Research and Testing, Berlin, Germany; and Ø. GRONG is with the Department of Materials Science and Engineering, Norwegian University of Science and Technology, Trondheim, Norway.*

tures for Sc, Fe, Mn, and Co are all within two deg of one another, whereas the Ni eutectic temperature is somewhat lower. The partition coefficients (k) shown in Table 1 were calculated assuming straight liquidus and solidus lines:

$$k = C_S / C_E \quad (1)$$

where C_S is the solute solubility at the eutectic temperature and C_E is the eutectic composition. These coefficients, although specifically meant for Al-X binary alloys, are used in this study for Al-Zn-Mg-X alloys assuming a high dilution of X impurity in aluminum. It is understood that this is only an approximation, making an assumption that Zn and Mg do not significantly alter the solubility of these impurity elements in aluminum.

In Fig. 2, the Scheil Equation has been used to calculate the quantity of nonequilibrium eutectic (f_E) generated in aluminum binary alloys as a function of solute content (C_0) using the data in Table 1:

$$f_E = (C_0 / C_E)^{1/1-k} \quad (2)$$

At normal impurity levels (i.e., less than 0.3 wt-%), Co and Sc are observed to generate the greatest amount of eutectic, followed by Fe and Ni. Mn, however, generates only a negligible amount of eutectic in this solute range.

Considering in more detail the effect of Fe on the solidification of 7108 requires knowledge of the Al-Zn-Mg-Fe quaternary system, which is not well documented. Mondolfo predicts three phases, $FeAl_3$, $Mg_3Zn_3Al_2$, and $MgZn_2$, for conditions where Zn:Mg > 2.2 and Fe >> Si (Ref. 9). From the Al-Zn-Mg ternary equilibrium system, one would expect to form $Mg_3Zn_3Al_2$ through a eutectic reaction starting below 489°C, followed by a peritectic reaction to form $MgZn_2$ at around 475°C. From examining Al-Zn-Fe and Al-Mg-Fe ternary equilibrium systems, it is to be expected that $FeAl_3$ will form at elevated temperatures close to the liquidus through a eutectic reaction. However, it has been well documented that $FeAl_6$ is more commonly observed in place of $FeAl_3$ for fast cooling rates (Ref. 10). Also, for fast cooling rates, the peritectic reaction to form $MgZn_2$ is not expected to occur to any significant extent. Hence in 7108 weld metal, $FeAl_6$ and $Mg_3Zn_3Al_2$ are the two intermetallic phases expected to form.

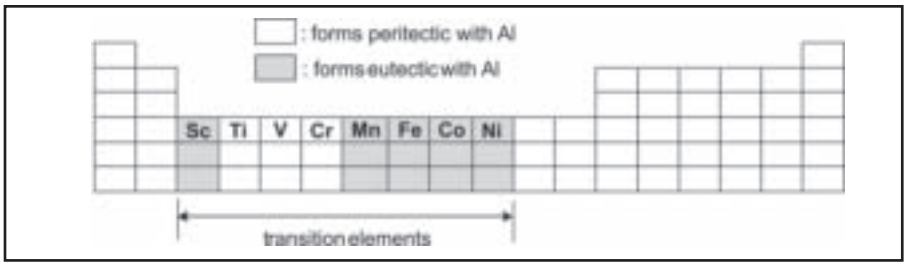

Fig. 1 — Periodic table showing transition elements pertinent to this study.

Aluminum Weldability

Solidification cracking is a defect common to many aluminum alloys, where susceptibility to this form of cracking is normally used to define weldability. Formation of this defect involves the separation and tearing of liquid films present at grain boundaries in the mushy zone trailing the weld pool. Recent models have suggested that crack initiation may arise from a pressure drop in the interdendritic liquid due to insufficient liquid feeding of solidification shrinkage and thermal contraction (Refs. 11–13). Accordingly, anything that inhibits interdendritic fluid flow should promote crack formation.

The link between liquid feeding and crack formation is being considered in this study to explain how interdendritic phases that form at high temperature and block interdendritic channels may influence weldability. Evidence that a high-temperature Fe-bearing phase can affect the pressure drop in solidification has been found in several aluminum castability studies, where it has been shown that shrinkage porosity increases with Fe impurity content (Refs. 14–16). Specifically, this effect has been related to coarse β-Al_5FeSi needles in Al-Si alloys that effectively block liquid feeding in interdendritic channels. Regarding solidification cracking susceptibility, however, Fe has actually been shown to have a positive effect in castings (Refs. 16–19), attributed in some cases to mechanical bridging between dendrites by the β phase. Such bridging is not possible in welds, however, where interdendritic phases are considerably finer in size and refined in shape. Instead of its traditional coarse needle shape spanning across dendrites in castings, the weld metal β phase is found to be refined in size and restricted to grain boundaries (Ref. 20).

Weld metal grain size can also have a pronounced effect on weldability (Refs. 5, 21). Grain refinement results in more weld metal grain boundaries, with less strain per grain boundary and more resistance to cracking (Ref. 22). Thus, any effect that impurity additions may have on weldability must include an analysis of grain size. Grain refinement involves the heterogeneous nucleation of new grains, which requires both undercooling and the presence of an appropriate substrate (Ref. 6). When the substrate is similar in crystal structure to the metal being nucleated, less undercooling is required. Constitutional undercooling can be related to alloy partitioning and compared using the parameter P (Ref. 23):

$$P = \frac{m_L(1-k)C_0}{k} \quad (3)$$

where m_L is the liquidus slope. Undercooling parameter values for the transition elements are compared in Table 2 (for $C_0 = 1$), where it is observed that Mn should generate the least amount of undercooling and Ni the highest.

Experimental

The effect of impurity elements Fe, Mn, and Co on the solidification cracking susceptibility of Alloy 7108 was studied by per-

Table 1 — Compilation of Phase Equilibrium Data for Select Transition Elements in Aluminum (Refs. 8, 9)

Solute	T_E Eutectic Temp (°C)	C_S Solubility at T_E (wt-%)	C_E Eutectic Comp. (wt-%)	C_I Inter-Metallic (wt-%)	k Partition Coefficient	Intermetallic Compound
Sc	655	0.31	0.6	35.7	0.52	$ScAl_3$
Mn	657	1.8	1.9	25.3	0.95	$MnAl_6$
Fe	655	0.04	1.8	37.0	0.022	$FeAl_3$
Co	657	0.02	1.0	32.7	0.020	Co_2Al_9
Ni	640	0.04	6.0	42.0	0.0067	$NiAl_3$

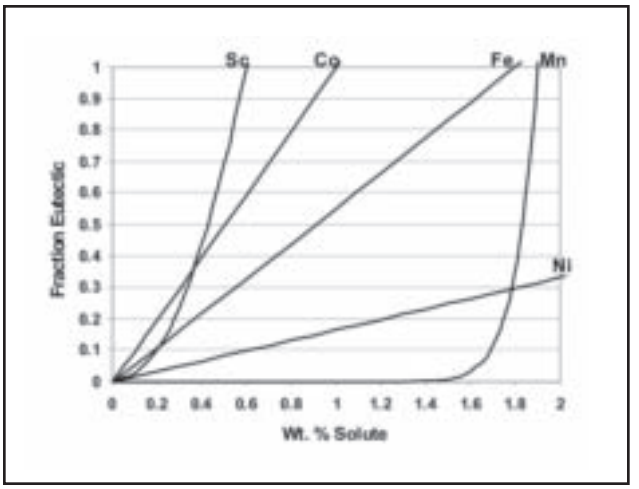

Fig. 2 — Graphical representation of Scheil Equation predictions for quantity of interdendritic eutectic in aluminum binary alloys based upon Equation 2 and Table 1.

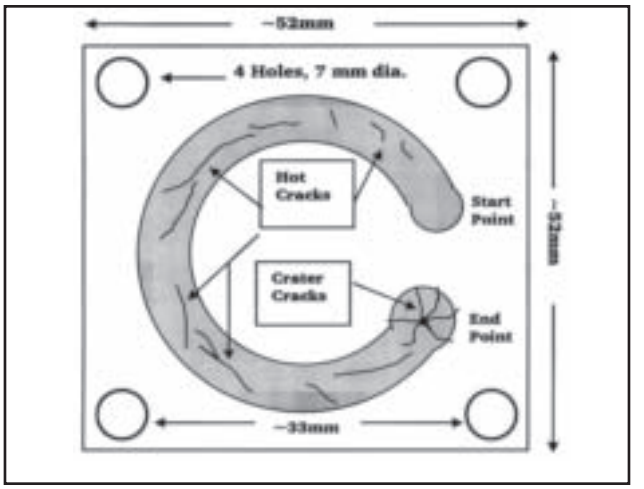

Fig. 3 — Schematic diagram showing coupon design used for CPT weldability test with crack pattern traced from Al-5½Zn-1Mg-0.2Fe specimen.

forming weldability tests on specially prepared cast coupons having variable impurity content. Details of the weldability test and alloy preparation are discussed below.

Weldability Testing

The CPT was developed for use in this study, specifically adapted for evaluating small cast coupons of experimental alloys (Ref. 3). There are numerous versions of this test as described in a review on this subject (Ref. 24), but the basic test consists of a weld made in a circular pattern on a flat plate. As the weld nears completion of the circle, it begins to experience transverse tensile strain from the weld bead made at the beginning of the circle. Thus, when welding susceptible alloys, a solidification crack (normally a centerline crack) will eventually form and trail behind the weld pool until the circle is completed. The total length of the crack generated can then be measured and used as an indication of relative weldability.

The CPT fixture developed for use in this investigation consisted of a coupon affixed to a water-cooled copper heat sink, mounted to the headstock of a rotary lathe. A stationary gas tungsten arc welding (GTAW) torch was mounted perpendicular to the head stock and was offset from the lathe centerline, so that a circular path of approximately 40 mm in diameter was traced as a result of coupon rotation. The CPT weld coupons were 10-mm-thick cast alloys (approximately 52 mm square) with four corner holes provided for mounting bolts, as shown schematically in Fig. 3. A heat sink was found necessary for these small coupons to avoid overheating and subsequent melt-through.

Weld Parameter Development

Circular patch test welds were made using an autogenous, gas tungsten arc, bead-on-plate process. In order to obtain a narrow weld bead with high penetration, welds were made using direct current and straight polarity (electrode negative) with welding-grade helium shielding gas. A set of CPT weld tests were conducted in an earlier study (Ref. 3) to develop an appropriate test procedure and determine the effect of welding process variables on solidification cracking. The variables examined included welding current and welding speed, with the diameter of the circle kept constant at 40 mm. Results indicated that the most effective (i.e., the most crack producing) range of parameter combinations was a current of 130 A combined with a travel speed of 3.5 mm/s. These parameters were similarly adopted for this study.

Crack Length Measurement

Quantitative crack length measurements were obtained by grinding and polishing the top surface of the welded specimen to a 3-µm grit finish. A digital caliper and a metallurgical light stereoscope, equipped with oblique lighting, were used to measure the total, accumulative length of cracks. The magnification range selected was in accordance with the best visibility of cracks and varied from 10 to 16×. Crater cracks and HAZ cracks were not included in crack length measurements.

Figure 3 is a schematic illustration of the way a typical specimen appeared under the stereoscope. A crack pattern has been traced onto this schematic from an actual test specimen (Al-5½Zn-1Mg-0.2Fe). Cracking is most severe in weld segments located near the corners of the coupon where high restraint is exerted due to fixturing (i.e., corner bolts), indicating that the imposed restraint on the specimens is nonuniform. Also, it should be noted that the crack pattern observed in this test is not the same as the pattern normally found in a CPT test (i.e., one long centerline crack at the end of the circular patch). However, because the restraining condition was the same for all specimens, the resulting crack length measurements still serve as a valuable solidification cracking index for comparative purposes.

CPT Validation

In order to validate the ability of the CPT test to correctly compare relative

Table 2 — Comparison of Grain Refining Parameters for Impurity Additions (for C_0=1) (Ref. 9)

Solute	$m_L(1-k)/k$ (°C/wt-%)	Intermetallic	Lattice Spacing (×10^{-10}m)
Sc	7	$ScAl_3$, cubic	a = 4.11
Mn	0.1	$MnAl_6$, orthorombic	a = 6.49, b = 7.54, c = 8.86
Fe	123	$FeAl_6$, orthorhombic	a = 6.49, b = 7.44, c = 8.79
Co	147	Co_2Al_9, monoclinic	a = 6.21, b = 6.29, c = 8.56
Ni	494	$NiAl_3$, orthorhombic	a = 6.61, b = 7.37, c = 4.81

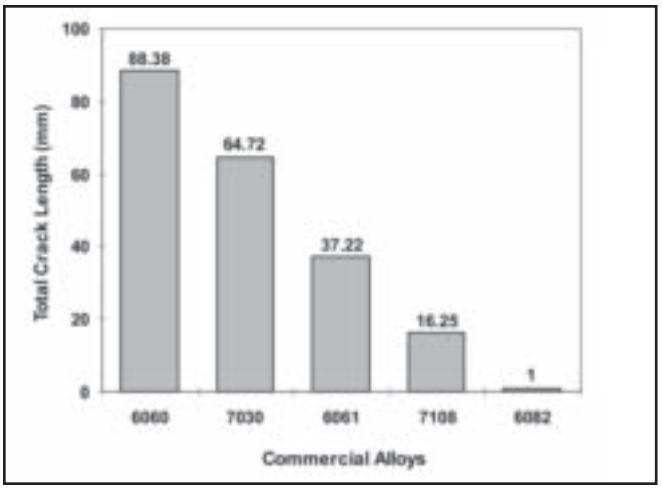

Fig. 4 — Circular patch test weldability analysis comparison of commercial aluminum alloys.

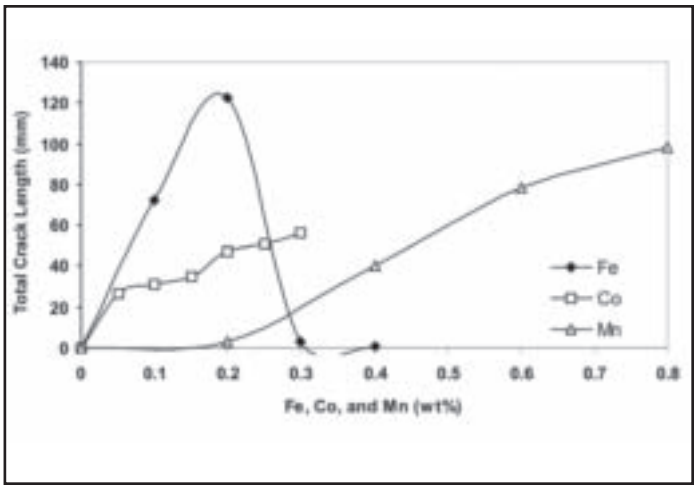

Fig. 5 — Circular patch test weldability data showing variations in total crack length (TCL) with Co, Fe, and Mn impurity additions to Al-5½Zn-1Mg alloy.

weldability, a series of CPT coupons were made from 5-mm-thick 6xxx and 7xxx aluminum alloy extrusions as listed in Table 3 (with the exception of Alloy 6061, which was cut from 7-mm-thick rolled plate). All materials were tested in the T6 temper. These coupons were welded autogenously using the same conditions and welding parameters discussed earlier for cast 7108 coupons. Alloys compared in such a way are shown in Fig. 4, where it is observed that the most susceptible alloy was 6060, and the least susceptible alloy was 6082. This agrees with industrial experience, where Alloys 6060 and 7030 are normally considered unweldable, whereas Alloys 7108 and 6082 are normally considered readily weldable when using a proper filler metal (Ref. 1).

Experimental Alloy Preparation

The experimental alloys examined in this study were prepared by adding preweighed amounts of impurity master alloys (Al-10Fe, Al-10Mn, and Al-5Co) to a high-purity Al-5½Zn-1Mg alloy. The Al-5½Zn-1Mg alloy was made to simulate Alloy 7108, prepared by adding Mg and Zn to 99.999 wt-% pure aluminum under a protective sulfur hexafluoride gas cover. The range of impurity additions made, compared in Table 4, shows values that extend beyond normal impurity limits.

Once an impurity master alloy was added to the molten Al-Zn-Mg alloy, the mixture was sparged with argon and then cast into a graphite book mold, precoated with boron nitride. Coupons were prepared for welding by rough grinding both sides of the coupon (800 mesh grit) followed by alcohol degreasing. Corner holes were dry machined with the aid of a template.

Metallography

In order to prepare CPT coupons for grain size evaluation, they were first ground and polished to 3-μm grit, followed by electro-etching and anodizing. The areas of interest were viewed using polarized light under a light microscope at an appropriate magnification. Grain size measurements in the castings were made using a line intercept method, calculating an average grain diameter over approximately 150 grain intercepts. Measurements in the weld were made from a top view, using a line intercept method across the full width of the fusion zone. Mean grain size values were used to represent the overall effect of a particular impurity element.

Results and Discussion

Weldability Measurements

Figure 5 gives the results of the CPT test, showing the variation of total crack length for different additions of Fe, Mn, and Co. What is readily apparent from this data is that Fe additions result in the highest amount of cracking. The crack length data for Fe is also unique in that it passes through a maximum, with cracking dropping to zero at around 0.3 wt-% Fe. This corroborates a reference made in the literature, where a high Fe content (0.3–0.4

Table 3 — Nominal Compositions for Commercial Aluminum Alloys Evaluated in CPT Validity Test (Refs. 4, 25)

Alloy	wt-%	Si	Fe	Cu	Mn	Mg	Cr	Zn	Zr	Other Total	Al
7030.60	min	—	0.15	0.26	—	1.10	—	5.10	—		
	max	0.10	0.25	0.34	0.04	1.30	0.03	5.40	0.03	0.10	bal
7108.70	min	—	—	—	—	1.10	—	5.30	0.15		
	max	0.12	0.20	0.05	0.04	1.30	0.03	5.60	0.18	0.10	bal
6060.35	min	0.40	0.18	—	0.01	0.45	—	—	—		
	max	0.45	0.22	0.02	0.03	0.50	0.02	0.02	—	0.10	bal
6061	min	0.40	—	0.15	—	0.80	0.04	—	—		
	max	0.80	0.70	0.40	0.15	1.20	0.35	0.25	—	0.10	bal
6082.26	min	0.85	0.17	—	0.50	0.60	0.13	—	—		
	max	0.95	0.23	0.01	0.60	0.65	0.18	0.02	—	0.10	bal

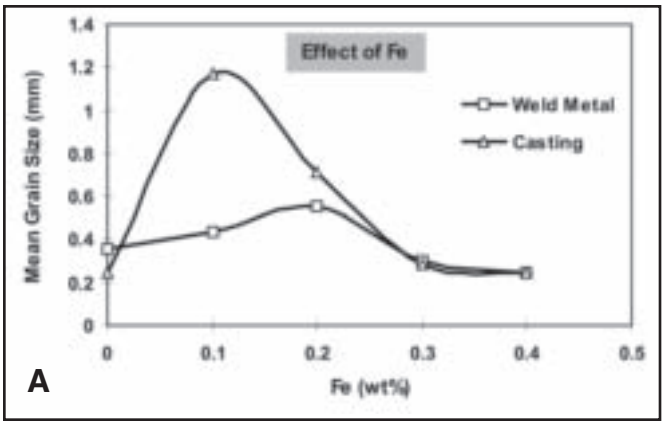

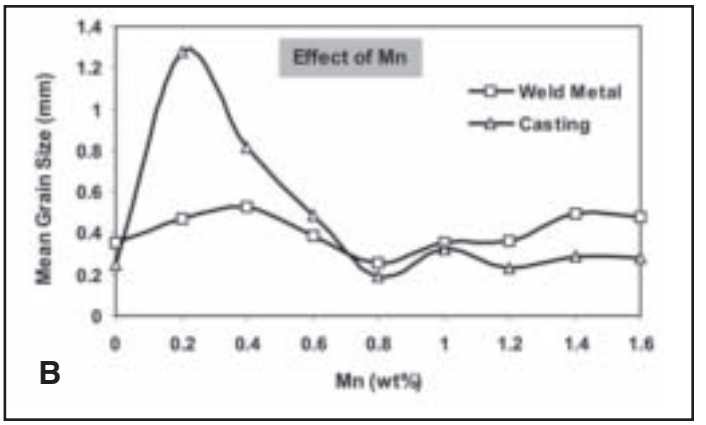

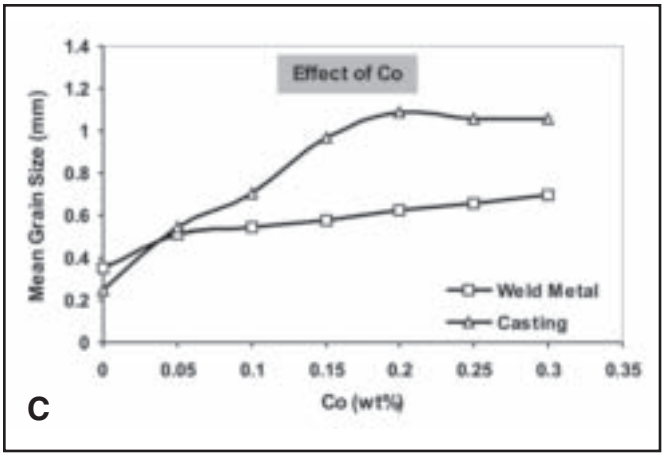

Fig. 6 — Effect of the following impurity additions on Al-5½Zn-1Mg weld metal and casting grain size: A — Fe, B — Mn, and C — Co.

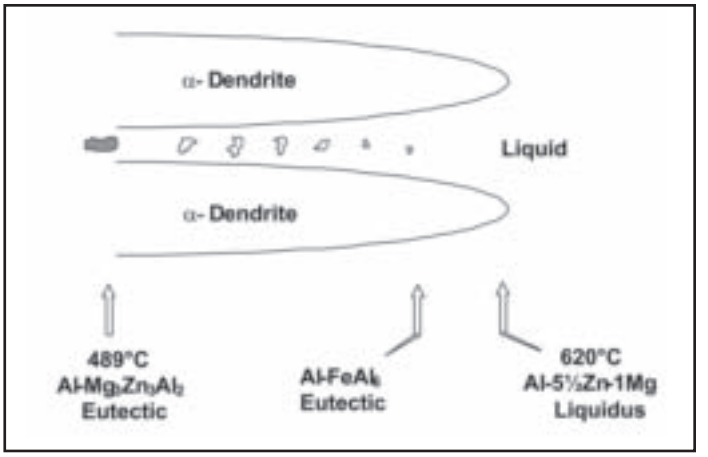

Fig. 7 — Schematic diagram showing phase-temperature sequence for Fe impurity in Al-5½Zn-1Mg alloy.

wt-% Fe) was reportedly found to be beneficial to the weldability of Alloy 7039 (Ref. 26). This improvement in weldability corresponds directly with a reduction in grain size, discussed below.

It should also be noted that cracking begins to occur for Fe and Co additions at a much lower solute content than for Mn additions. This follows from the fact that much larger quantities of Mn are required to generate the same quantity of eutectic (Fig. 2). If a certain volume fraction of eutectic is required to impede interdendritic flow, it makes sense that more Mn must be added before hot cracking will initiate. Additions of Mn above 0.8 wt-%, although not shown in Fig. 5, resulted in a plateau of about 95 mm total crack length (up to 1.4 wt-% Mn). Mn behaved uniquely in a second regard, in that it was the only impurity addition that resulted in severe HAZ cracking. However, these HAZ cracks were not included in the total crack length count.

Grain Size Comparison

Grain size measurements were taken for all welds, and their corresponding castings, for each CPT coupon. The results of these evaluations are presented in Fig. 6, where it is noted that two modes of behavior are observed. Both Fe and Mn additions result in a peak in grain size, whereas Co results in a continuous rise in grain size for welds and castings. For all additions, however, the weld metal grain size rests below or is approximately the same as the casting grain size. This is to be expected due to the higher growth rates, and hence higher undercooling, associated with welding. Actual cooling rate measurements, made using implanted thermocouples, showed the weld to cool at 280°C/s and the casting to cool at 19°C/s during solidification. Also, the weld metal grain size is to some extent influenced by the casting grain size due to the tendency for epitaxial grain nucleation.

The average grain diameter for welds and castings with no impurity addition is between 0.2 and 0.4 mm. By making small amounts of impurity additions (Fe, Mn, or Co), the casting grain diameter is found to increase up to around 1.2 mm. One explanation for this dramatic increase in grain size may be related to the eutectic heat of fusion, evolved near the solidification interface where grain nucleation is expected to occur.

If the impurity eutectic latent heat of fusion is to blame for inhibiting grain refinement for Fe, Mn, and Co, some other mechanism must account for the drop in grain size observed at high levels of Fe and Mn. From Equation 3 it is clear that undercooling increases with solute content and, hence, this may explain the observed refinement. Even so, Fe and Co are both capable of producing higher undercooling than Mn, for a given impurity content, and yet Mn showed grain refinement and Co not. It is also possible that particles of these eutectic compounds may serve as substrates to nucleate new grains, although none of these compounds (from Table 2) appear to be suitable substrates. Only $ScAl_3$ has a crystal structure and lattice spacing close to that of aluminum (Al: a = 4.05×10^{-10} m, FCC).

Table 4 — Range of Impurity Additions Made to Al-5½Zn-1Mg Alloy (in wt-%)

Fe	0.05	0.10	0.15	0.20	0.25	0.30	0.40	
Mn	0.20	0.40	0.60	0.80	1.00	1.20	1.40	1.60
Co	0.05	0.10	0.15	0.20	0.25	0.30		

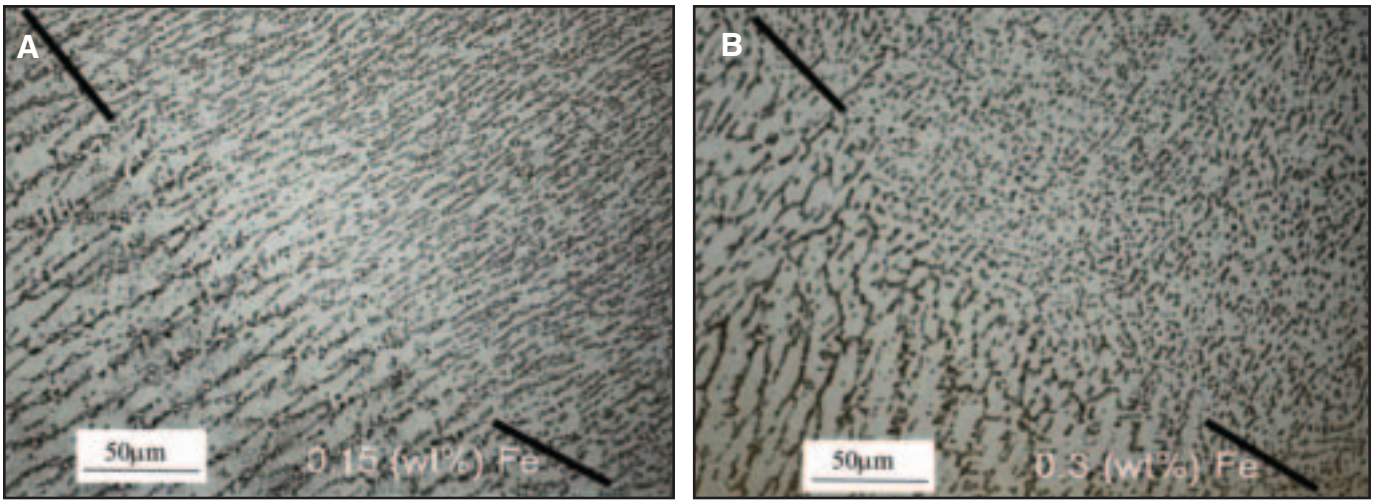

Fig. 8 — Photomicrographs showing cross section through quenched weld pool for Al-5½Zn-1Mg alloy treated with the following: A — 0.15 wt-% Fe and B — 0.30 wt-% Fe. Heavy line demarks boundary between normal and quenched weld metal.

Microstructure Development

The Al-5½Zn-1Mg weld metal solidification microstructure consists of primary aluminum dendrites and a discontinuous, interdendritic eutectic second phase. This eutectic second phase has been determined to consist primarily of the $Mg_3Zn_3Al_2$ phase (Refs. 2, 27). According to ternary phase equilibria, the liquidus for this alloy is approximately 620°C and the $Mg_3Zn_3Al_2$ eutectic occurs around 489°C (Refs. 9, 28). When iron is added in small amounts, an additional phase is observed intermixed with the $Mg_3Zn_3Al_2$ phase, identified in this study as $FeAl_6$ using SEM-EDX analysis. The order of phase formation, depicted schematically in Fig. 7, has the $FeAl_6$ phase forming close below the 620°C liquidus temperature, providing the possibility for interference with liquid feeding and disruption in growth of the $Mg_3Zn_3Al_2$ phase.

Metallographic examination of the Al-5½Zn-1Mg weld metal for both low and high Fe content revealed little noticeable difference. The prevalent interdendritic $Mg_3Zn_3Al_2$ phase, although discontinuous, tends to be elongated in the direction of solidification. When solidification takes place at higher growth rates, however, a change in behavior is observed. This is demonstrated in Fig. 8, where weld pool quenching was achieved by extinguishing the arc with a blast of pressurized air. In the rapidly cooled zone, the interdendritic phase is seen to be divided into smaller, more spherical particles for the specimen with high Fe content. This suggests that the Fe eutectic has the tendency to disrupt the growth of the $Mg_3Zn_3Al_2$ phase.

Summary

Sc, Mn, Fe, Co, and Ni transition elements, when present at impurity levels in aluminum and aluminum alloys (e.g., 7108), are unique in that they all solidify as eutectics at high temperature near the liquidus. The formation of eutectic early in the solidification sequence, near the dendrite tip, can have both positive and negative consequences. Interdendritic fluid flow is likely obstructed when high temperature eutectic is present, inhibiting the feeding of shrinkage and promoting the formation of porosity and solidification cracks. Adding to this negative effect on weldability is an increase in grain size associated with the release of latent heat near the dendrite tip. Countering these negative effects, however, is grain refinement that can occur at elevated impurity levels due to constitutional undercooling or the presence of a potent nucleating substrate.

How these different factors interact to influence 7108 weldability varies depending upon the particular element in question. Sc is known to be an effective grain refiner due to its eutectic compound serving as a potent nucleant. Compared to the other transition elements, Sc is unique in this regard. Both Mn and Fe additions resulted in grain refinement, but only at elevated impurity levels related to constitutional undercooling. Considerably more Mn is needed to achieve the same grain refinement, as reflected in its lower undercooling parameter. Fe additions showed improved weldability with grain refinement, whereas Mn did not. This difference in behavior may reflect upon the ability of the corresponding eutectic to block feeding, although Mn should generate less eutectic at the same impurity level. A more plausible explanation may be linked to HAZ cracking, observed only with Mn additions, where HAZ cracks could serve to initiate weld metal cracks.

Co did not produce any grain refinement even though its undercooling parameter is similar to that of Fe. Co additions resulted only in grain coarsening and a corresponding decrease in weldability. Ni additions, although not examined in the experiment, give the highest undercooling parameter and hence show potential for promoting grain refinement.

The role of Fe on 7108 weldability is of particular practical importance because of its natural occurrence as an impurity element. A peak in solidification cracking susceptibility has been observed to occur at approximately 0.2 wt-% Fe, which coincides with the typical Fe impurity level for commercial alloys. Controlling Fe is problematic, because restricting Fe to lower levels becomes cost prohibitive, whereas adding Fe to higher levels leads to poor toughness and reduced corrosion resistance. A more favorable approach may be to control the impurity Si, and hence its interaction with Fe, to avoid formation of the high-temperature $FeAl_6$ eutectic. This is a topic for future research.

Acknowledgments

The authors are grateful to the Norwegian Aluminium-in-Ships program for sponsoring this work. Special thanks are given to Hydro Aluminium for the generous donation of materials and SINTEF for providing technical support.

References

1. Mousavi, M. G., Cross, C. E., Grong, Ø., and Hval, M. 1997. Controlling weld metal dilution for optimized weld performance in aluminium. *Science and Technology of Welding and Joining* 2(6): 275–278.

2. Cross, C. E., and Grong, Ø. 1998. Microstructural and mechanical properties of simulated Al-Mg-Zn weld metal modified with Sc and Zr. *Proc. ICAA-6 Aluminum Alloys Conf.*, 1441–1446. Eds. T. Sato, S. Kumai, T. Kobayashi, and Y. Murakami. Japan Inst. Light Metals.

3. Mousavi, M. G., Cross, C. E., and Ramsland, A. R. 1997. Development of a patch weldability test for evaluating hot cracking in aluminium weldments. *Report No. STF24-F97712*. SINTEF. Trondheim, Norway.

4. Aluminium Alloy Specifications, Roufoss Hydro Automotive Research Center AS, Raufoss, Norway.

5. Mousavi, M. G., Cross, C. E., and Grong, Ø. 1999. Effect of scandium and titanium-boron on grain refinement and hot cracking of aluminium Alloy 7108. *Science and Technology of Welding and Joining* 4(6): 381–388.

6. Crossley, F. A., and Mondolfo, L. F. 1951. Mechanism of grain refinement in aluminum alloys. *Trans. AIME* 191(12): 1143–1148.

7. Norman, A. F., Prangnell, P. B., and McEwen, R. S. 1998. The solidification behaviour of dilute aluminium-scandium alloys. *Acta Materialia* 46: 5715–5732.

8. Gschneider, K. A., and Calderwood, F. W. 1989. Aluminum-scandium. *Bulletin of Alloy Phase Diagrams* 10: 34.

9. Mondolfo, L. F. 1976. *Aluminum Alloys: Structure & Properties*. London: Butterworth.

10. McL. Adam, C., and Hogan, L. M. 1972. The aluminium-iron eutectic system. *J. Australian Inst. Metals* 17(2): 82–90.

11. Feurer, U. 1977. Influence of alloy composition and solidification conditions on dendrite arm spacing, feeding and hot tearing properties of aluminium alloys. *Proc. Symp. on Quality Control of Engineering Alloys and the Role of Metals Science*, 131–145. Eds. H. Nieswag and J. W. Schut. Delft.

12. Rappaz, M., Drezet, J. M., and Gremaud, M. 1999. A new hot-tearing criterion. *Met. Mat. Trans.* 30A: 449–455.

13. Coniglio, N. 2008. Aluminum alloy weldability-identification of weld solidification cracking mechanisms through novel experimental technique and model development. Doctoral thesis dissertation, Otto-von-Guericke Universität, Magdeburg, BAM Pub., Berlin.

14. Eklund, J. E. 1991. On the effects of impurities on the solidification and casting of aluminium alloys. PhD thesis dissertation, Helsinki Univ. of Tech, Helsinki, Finland.

15. Taylor, J. A., Schaffer, G. B., and StJohn, D. H. 1999. The role of iron in the formation of porosity in Al-Si-Cu-based casting alloys: Part III. A microstructural model. *Met. Mat. Trans.* 30A(6): 1657–1662.

16. Lu, L., and Dahle, A. K. 2005. Iron-rich intermetallic phases and their role in casting defect formation in hypoeutectic Al-Si alloys. *Met. Mat. Trans.* 36A(3): 819–835.

17. Couture, A. 1981. Iron in aluminum casting alloys — A literature survey. *AFS Int. Cast Metals J.* 6(4): 9–17.

18. Singer, A. R. E., and Jennings, P. H. 1947. Hot-shortness of some aluminium-iron-silicon alloys of high purity. *J. Inst. Metals* 73: 273–284.

19. Mbuya, T. O., Odera, B. O., and Ng'ang'a, S. P. 2003. Influence of iron on castability and properties of aluminium silicon alloys — Literature review. *Int. J. Cast Metals Research* 16(5): 451–465.

20. Coniglio, N., and Cross, C. E. 2008. Effect of cooling rate and silicon content on solidification path and phase constituents in 6060 aluminum castings and weld metal. *Proc. 11th Int. Conf. on Aluminium Alloys*, 1889–1896. Deutsche Gesellschaft für Materialkunde.

21. Dvornak, M. J., Frost, R. H., and Olson, D. L. 1989. The weldability and grain refinement of Al-2.2Li-2.7Cu. *Welding Journal* 68(8): 327-s to 335-s.

22. Spittle, J. A., and Cushway, A. A. 1983. Influences of superheat and grain structure on hot tearing susceptibilities of Al-Cu alloy castings. *Metals Technology* 10: 6–13.

23. Tarshis, L. A., Walker, J. L., and Rutter, J. W. 1971. Experiments on the solidification structure of alloy castings. *Met. Trans.* 2(9): 2589–2597.

24. Nelson, T. W., Lippold, J. C., Lin, W., and Baeslack III, W. A. 1997. Evaluation of the circular patch test for assessing weld solidification cracking, Part I — Development of a test method. *Welding Journal* 76(3): 110-s to 119-s.

25. *Aluminum Standards and Data*. 1984. Washington, D.C.: Aluminum Association.

26. Gibbs, F. E. 1966. Development of filler metals for welding Al-Zn-Mg Alloy 7039. *Welding Journal* 45(10): 445-s to 453-s.

27. Liang, H., Chen, S. L., and Chang, Y. A. 1997. A thermodynamic description of the Al-Mg-Zn system. *Met. Trans.* 28A(9): 1725–1734.

28. Phillips, M. A. 1959. *Annotated Equilibrium Diagrams of Some Aluminium Alloy Systems*. Monograph and Report Series No. 25. London: The Institute of Metals.